EUROPEAN ORGANIZATION FOR NUCLEAR RESEARCH
European Laboratory for Particle Physics

Large Hadron Collider Project

LHC Project Report 313

Experimental Investigations of the Electron Cloud Key Parameters

V.V. Anashin[3], V. Baglin[1], R. Cimino[2], I.R. Collins[1], R.V. Dostovalov[3], N.V. Fedorov[3], J. Gómez-Goñi[1*], O. Gröbner [1], B. Henrist[1], N. Hilleret[1], A.A. Krasnov[3], J–M. Laurent[1], O.B. Malyshev[3], E.E. Pyata[3] and M. Pivi[1]

1 CERN, LHC Division
2 INFN, Trieste, Italy
3 BINP, Novosibirsk, Russia
* Financial support by the Spanish Secretary of the Universities and Research, grant number PR99/0009354327

Presented at e^+e^- Factories '99
International Workshop on Performance Improvement of Electron-Positron Collider Particle Factories
21-24 September 1999, KEK, Tsukuba, Japan

Administrative Secretariat
LHC Division
CERN
CH - 1211 Geneva 23
Switzerland

Geneva, 18 October 1999

EXPERIMENTAL INVESTIGATIONS OF THE ELECTRON CLOUD KEY PARAMETERS

V. Baglin, I.R. Collins[†], J. Gómez-Goñi[*], O. Gröbner, B. Henrist, N. Hilleret, J–M. Laurent, M. Pivi, CERN, Geneva, Switzerland
R. Cimino, INFN, Trieste, Italy
V.V. Anashin, R.V. Dostovalov, N.V. Fedorov, A.A. Krasnov, O.B. Malyshev, E.E. Pyata, BINP, Novosibirsk, Russia

Abstract

Motivated by a potential electron cloud instability and the possible existence of electron multipacting in the LHC vacuum system, that may result in additional gas desorption and unmanageable heat loads on the cryogenic system, an extensive experimental research program is underway at CERN to quantify the key parameters driving these phenomena. Parameters, such as: photoelectron yield, photon reflectivity, secondary electron yield etc from industrially prepared surfaces have been quantified. In addition to their dependenceon photon dose the effect of temperature and presence of external fields has also been studied.

1 INTRODUCTION

The build up of an electron cloud and electron multipacting was first observed in the ISR over two decades ago [1]. There electrons, generated by beam ionisation of the residual gas, were accelerated by the electric field of successive bunches towards the vacuum chamber wall. The signature for electron multipacting was the very fast increase in pressure due to electron stimulated desorption in a specific location of the machine where an aluminium vacuum chamber had been installed. This local pressure rise had detrimental effects on the operation of the machine. Multipacting occurred due to the larger secondary electron yield of aluminium as compared with that of stainless steel used elsewhere in the machine. In the LHC the main source of electrons will be from photoelectrons generated from the walls of the vacuum chamber when irradiated with synchrotron radiation.

The phenomenon of multipacting in the LHC may be understood from the schematic depicted in Figure 1.

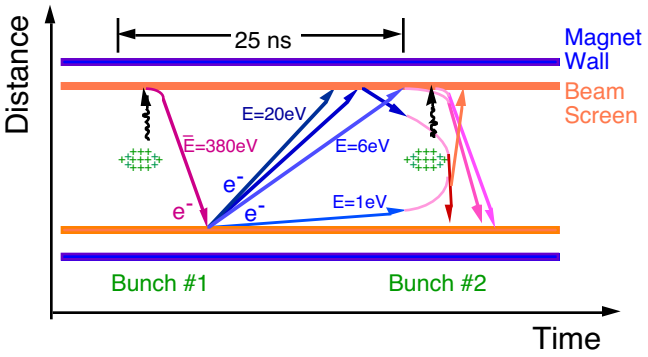

Figure 1: A simplified view of the evolution (radial distance versus time) of an electron cloud at a given location along a line defined by the intersection of the horizontal and transverse vertical cross–sectional planes of the beam screen.

Synchrotron radiation, with a critical energy of 44.1 eV, impinges on the beam screen in the contemporary presence of the proton bunch from which it was emitted (a single photon is shown in the figure for clarity). The photons may be reflected, to be absorbed elsewhere, or electrons may be emitted that traverse the vacuum chamber and impact the opposite wall with an average energy of 380 eV, depositing power onto the beam screen and/or perhaps desorbing gas molecules (not shown). Alternatively a number of secondary electrons may be created with a kinetic energy distribution from 0 eV up to the incident electron energy, however predominately weighted at the low energies. These electrons drift across the vacuum. Electrons with an energy greater than about 6 eV impact the opposite wall of the beam screen before the arrival of the following bunch and may either be absorbed or may be reflected from the wall. All electrons remaining in the vacuum chamber and those generated when the following bunch

[†] Email: Ian.Collins@CERN.CH
[*] Financial support by the Spanish Secretary of the Universities and Research, grant number PR99/0009354327

arrives are acceleratedtowards the bunch. Those close to the bunch experience a larger kick than those further out and impact the wall adding to the heat load on the beam screen.

Initial theoretical studies highlighted the concern of the heat loads generated by an electron cloud and electron multipacting in the cryogenic LHC vacuum system [2,3]. More recent simulations [4,5] have confirmed these initial concerns and have identified the sensitivity of the input parameters to the expected heat loads. The results of the intensive research program at CERN were reported on the data existing at that time and proposed possible solutions to avoid the fast build–up of an electron cloud [6]. An extensive bibliography of the studies for the LHC can be found on the Internet [7].

The electron cloud key parameters, such as photon flux, photon reflectivity, photoelectron yield, secondary electron yield and the effect of external magnetic fields are addressedin detail in the following sections. Parameters, such as beam screen shape and diameter, the bunch spacing, the bunch intensity, space charge, are not addressedhere since they have been addressedin previous studies [8]. Finally multipacting tests performed in the laboratory with a coaxial cavity are described. These experiments have proved useful to determine the effect of surface conditioning, such as bake-out, scrubbing with electrons, treatment with a freon11 discharge and the effect of an external solenoid field.

2 KEY PARAMETERS

2.1 Photon flux

The photon flux is a key parameter for the electron cloud in the LHC since the emitted synchrotron radiation generated by the circulating protons may create photoelectrons when adsorbed by the vacuum chamber wall. At 7 TeV and at nominal beam current of 0.561 mA synchrotron radiation with a critical energy of 44.1 eV and a linear photon flux of 10^{17} photon/(s.m) irradiates the LHC beam screen. In Table 1 the linear photon fluxes and critical energies in the LHC are compared with those in LEP2.

Table 1: Comparison of the linear photon fluxes and critical energies in LEP2 and LHC.

	LEP2 E=100 GeV, I=6 mA	**LHC** E=7 TeV, I=0.561 mA
Linear photon flux (photons/(s.m))	$2.77 \cdot 10^{16}$	$9.87 \cdot 10^{16}$
Critical Energy (eV)	796 000	44.1

2.2 Photon reflectivity

Two independent studies, at EPA in CERN [9] and at VEPP–2M in BINP [10,11], have been performed to determine the photon reflectivity of prototype LHC beam screen surfaces. Photons with a critical energy of 45 and 194eV and 285 eV were incident at a mean incidence angle of 11 mrad and 20 mrad, respectively. The forward–scatteredphoton reflectivity was determined from the ratio of the photoelectron current generated on a collector after photon reflection from the chamber under examination and that generated under direct irradiation, *i.e.* without reflection. The results of the former study on Cu based surfaces are summarised in Table 2. The saw–tooth structure exhibits near vertical facets, designed to inhibit forward–scatteredreflection. Indeed, this surface indicated the lowest measured forward scattered photon reflectivity, with a generated photoelectron current close to the experimental sensitivity. The BINP study indicated similar results although performed under slightly different experimental conditions. Interestingly, there it was possible to measure the forward scattered reflection, not only as a ratio of the generated photoelectron current but also of the deposited power using a simple calorimetric collector. These latter measurements indicate a substantially lower forward-scattered reflectivity. The significantly different results found by the two means can be reconciled with the different photon energy sensitivities of the two methods. For a given incidence angle, the higher energy photons are preferentially adsorbed, *i.e.* the photon reflectivity is strongly photon energy dependent.

2.3 Photoelectron emission

The photoelectron yield most relevant to an accelerator physicist is the photoelectron yield per absorbed photon, Y*. By measuring locally the photoelectron current on a wire electrode and determining the photon reflectivity, R, as described in the previous section, it is possible to estimate the photoelectron yield per adsorbed photon. Assuming that all reflected photons are eventually absorbed with the same yield then the yield per absorbed photon, Y*, and per incident photon, Y, are simply related by:

$Y^* = Y/(1-R)$

The results, taken with a photon critical energy of 45 eV and a mean incidence angle of 11 mrad, for various prototype LHC beam screens are given in Table 2 [9]. There it can be seen that the lowest Y* is obtained for the saw–tooth material since the grazing incident synchrotron radiation impinges the structure close to normal incidence.

Table 2: Forward scattered photon reflectivity and photoelectron yield per incident (Y) and adsorbed (Y*) photon at 11 mrad mean incidence angle for various Cu surfaces taken with a 45 eV photon critical energy [9].

Material	R (%)	Y (e^-/photon)	Y* (e^-/photon)
OFE Cu	80.9	0.022	0.114
Air baked OFE Cu	21.7	0.075	0.096
Electroplated Cu	5.0	0.080	0.084
Saw–tooth Cu	1.8	0.052	0.053

2.3.1 The effect of magnetic fields

The effect of a dipole field on photoelectron emission has been studied at CERN [9] for normal incidence irradiation and at the BINP [10, 12] for normal and grazing incidence irradiation. In the former study it was shown that a relatively weak dipole magnetic field, approximately 0.1 T to be compared with the 8.33 T in the LHC, aligned parallel to the surface suppresses the photoelectron emission by more than two orders of magnitude. The photoelectron current was found to increase linearly with increasing electric bias and by extrapolating the data a bias of 42 keV would have to be applied to the collector to completely cancel the effect of the 0.1 T dipole field. In addition it was found that the attenuation factor was sensitive to the alignment of the surface to the magnetic field.

The latter study extended these observations by studying the field and alignment dependence of the photoelectron current. It was found that the photoelectron current decayed exponentially over two orders of magnitude reaching a saturation value at about 0.4 T. This strong attenuation is however reduced as the angle between the surface and the direction of the dipole field increases reaching a factor of attenuation of ten for a 1.5˚ misalignment. An experiment was also performed at grazing incidence as a function of dipole field strength from 4 strips, 2 flat strips top and bottom and 2 curved strip left and right, of prototype beam screen material [10]. This geometry closely resembles that in the LHC except that the maximum field strength of 0.3 T was attainable and the experiments were performed at room temperature. The photoelectrons emitted from the surfaces are constrained to travel along the field lines. Those from the curved strips, left and right, return to the same curved strip, thus generating no net current, and hence do not cross the centre of the vacuum chamber. In the case of the LHC these electrons will neither interact with the beam nor gain significant energy from the beam. The current from the flat strips top and bottom are not affected by the magnetic field.

The effect of an external solenoid field was studied using the laboratory multpacting tests discussed in section 3.4.

2.3.2 The effect of cryogenic temperatures and pre–condensed gases.

The effect on the photoelectron emission on cooling a prototype beam screen material and subsequently pre–condensing various gases at cryogenic temperatures has been studied. At grazing incidence, with a 285 eV photon critical energy, the photoelectron current is reduced by a factor of 1.4 on cooling the surface to 77 K and by a further factor of 1.2 and 3.4 on dosing with 100 monolayers or 1000 monolayers of CO_2 respectively [13]. A monolayer corresponds to approximately 10^{15} molecules/cm^2. At normal incidence the photoelectron current from pre–condensed layers of H_2, CH_4, CO, CO_2 and Ar at 3 K, 4.2 K, 4.2 K, 68 K and 4.2 K, respectively, remained approximately constant for a coverage up to ~100 monolayers [14]. In general, at higher coverages the photoelectron emission decreases with coverage.

2.3.3 The effect of photon dose

In the context of a potential electron cloud in the LHC, photoelectron yields were first studied at BESSY in Berlin using a VUV monochromated beamline [15]. In a similar following study the photoelectron yield, Y, and the energy dependence of the emitted electrons as a function of photon dose were investigated from a number of candidate materials for the LHC vacuum system [16]. It was found that after a high photon dose the measured photoelectron yields of all the different samples studied (without conditioning, such as bakeout, annealing or ion bombardment) were similar. It was proposed that photocracking of the native surface oxide, found on industrial surfaces, produces similar fragments left behind on the surface after the large photon dose. The results from a prototype LHC beam screen sample are shown in Figure 2. There is can be seen that, firstly, the spectrum is dominated by low energy electrons, presumable secondary electrons and, secondly, that the photon dose not only reduces the measured Y but significantly alters the emitted electron energy distribution, pushing it to higher energies. From the energy distribution it is tempting, therefore, to infer that the secondary electron yield, discussed in the following section, will be reduced in a similar manner with photon dose.

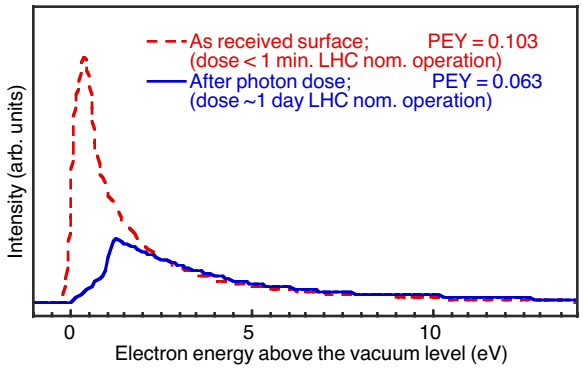

Figure 2: Energy distributions of electrons emitted at 45° from the surface for normal incident 'white light' from OFE Cu, a prototype LHC beam screen material, for a low and high LHC equivalent photon dose, taken from [15].

Recent photon scrubbing studies in EPA [17] and BINP [12] using a photon critical energy of 194 eV and 285 eV, respectively, at normal incidence on an OFE Cu roll-bonded on stainless steel sample, indicate that the photoelectron yield obeys a $D^{-0.12}$ law. Here D is the photon dose in the range 10^{18} to 10^{22} photons. Experiments are underway to determine the effect of pre–cleaning on the photon dose dependence of the photoelectron yield. Preliminary results seem to suggest that only the initial photoelectron yields at a relatively low photon dose are dependent on the pre–cleaning. These findings are in agreement with previous studies [15] and in particular are consistent with room temperature photon stimulated gas desorption yields as a function photon dose [18].

2.4 Secondary electron emission

There exists a universal curve describing secondary electron emission of metals at normal incidence. The secondary electron yield can be characterised by two parameters: the primary electron energy at which the yield is maximum, E_{max}, and the maximum yield, δ_{max}. These parameters depend strongly on the composition and surface roughness thus it is important to perform measurements on the technical surfaces proposed for the LHC beam screen. Such curves for a prototype LHC beam screen material are shown in Figure 3 where E_{max}=300 eV and δ_{max}=2.3±0.1 before electron bombardment and E_{max}=450 eV and δ_{max}=1.2 after scrubbing with an electron dose of $5{\cdot}10^{-3}$ C/mm^2 at 500 eV [19]. Clearly the secondary electron emission is strongly dependent on the conditioning of the surface.

If one analyses the energy distribution of the emitted electrons then one finds that the electrons have predominantly low energies (< 20eV). However, there exists an elastically back-scattered component in the spectrum corresponding to the reflection of the primary electrons. The reflectivity of electrons from the beam screen was included in recent simulations [5] showing that heat loads in the dipole magnets of the LHC may increase by a factor of 2.5 due to this effect.

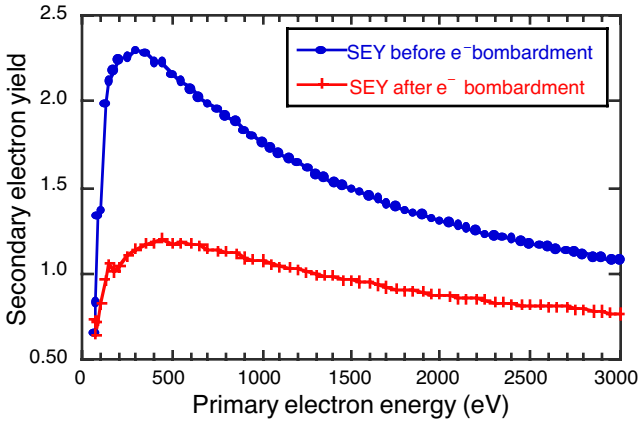

Figure 3: The variation of the secondary electron yield as a function of primary electron energy, for a sample of Cu co-laminated on stainless steel, before and after 5 mC/mm^2 electron bombardment with 500 eV electrons [19].

3 MULTIPACTING TESTS

3.1 Experimental set-up

Beam-induced multipacting is investigated in the laboratory by means of a travelling-wave, coaxial chamber with a base pressure of $5{\cdot}10^{-8}$ Torr. The electric field generated by the bunched proton beam in the LHC is simulated in the cavity by short square RF pulses applied to six equally spaced parallel wires inside a 100 mm diameter, 1.4 m long stainless steel vacuum chamber. The output from an amplifier, driven by a pulse generator, has no DC component and a bias voltage is applied to the wires in order to shift the pulses to the desired voltage. The power leaving the chamber is adsorbed in line loads.

Electrons close to the cavity wall are accelerated towards the centre of the cavity by the pulsed electric field. They may reach the opposite side of the chamber and produce secondary electrons. Resonance conditions are fulfilled if the following pulse arrives as the secondary electrons are emitted and as a result the electron cloud may grow exponentially. A positively biased electron pick-up, consisting of a 1 cm diameter button probe, is used to monitor the generated electron multipacting. Additional evidence of the existence of multipacting in the chamber is provided by a fast pressure increase. For a given pulse amplitude of 140 V and a period of 20 ns, multipacting is observed in a window of pulse widths between 7 and 16 ns. A similar behaviour is measured for the same

pulse amplitude and a fixed width of 10 ns, in a window of pulse periods between 17 and 22 ns.

3.2 The minimum pulse amplitude as a function of surface conditioning.

Once multipacting has been triggered the electron current on the probe is observed to decrease exponentially with time. Surface conditioning due to electron scrubbing results in a reduction of the secondary electron yield. Consequently the pulse amplitude has to be increased, as seen in Figure 4, so that the energy gained by the electrons also increases thus restoring a secondary electron yield sufficient to cause multipacting. After bake–out of the chamber the minimum pulse amplitude required to trigger multipacting is increased by a factor of 1.5. In addition the same cleaning efficiency, as compared with bake–out, is achieved with one order of magnitude less electron dose.

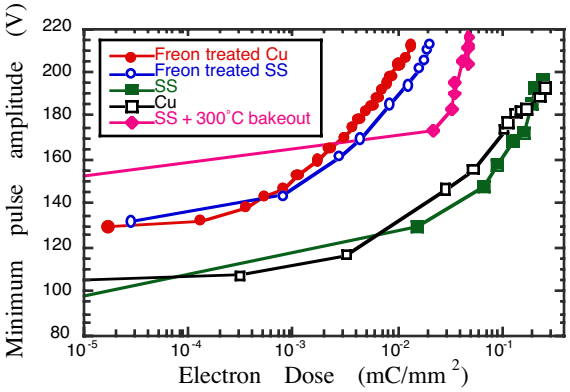

Figure 4: Minimum pulse amplitude required for multipacting as a function of the integrated electron dose: Stainless steel and copper before bake-out (lower curves) or after bake-out at 300˚C (St. Steel). Conditioning after Freon11 plasma and after venting to air for one week (upper curves).

If the system is left under vacuum for a few hours, following a high electron dose, the multipacting threshold decreases and re-conditioning is then slightly faster. Furthermore venting to pure O_2 for 24 hours was not effective in increasing the electron current on the probe. When vented to air for a few days current on the probe returns to its original value.

A freon11 vapour RF discharge treatment is found to be very effective in eliminating multipacting, both on stainless steel and copper surfaces, as shown in Figure 4. Preliminary tests show that a surface treatment can be achieved by leaking freon11 vapour (CCl_3F) inside the chamber for a few minutes during the multipacting discharge [20]. Remarkably, there is little degradation of the surface even after venting the chamber to air as shown in Figure 4. Auger electron spectroscopy analysis indicates a large carbon concentration (74%) on stainless steel samples exposed to the freon11 plasma. Copper samples exposed to the freon11 plasma contain chlorine in the bulk (up to 300Å) and no oxygen was observed.

3.3 Auger electron spectroscopy of samples exposed to multipacting.

Stainless steel samples exposed to different electron doses during multipacting have been analysed by means of Auger electron spectroscopy. The results shown in Figure **5** indicate that the relative carbon atomic concentration on the surface increases during electron bombardment while that of oxygen decreases. Although these are relative measurements one may infer that both effects occur since the iron concentration remains essentially constant. A possible explanation for this effect is that the residual hydrocarbons on the surface are decomposed by cracking due to the energetic multipacting electrons leaving a carbon rich surface exhibiting a low secondary electron yield.

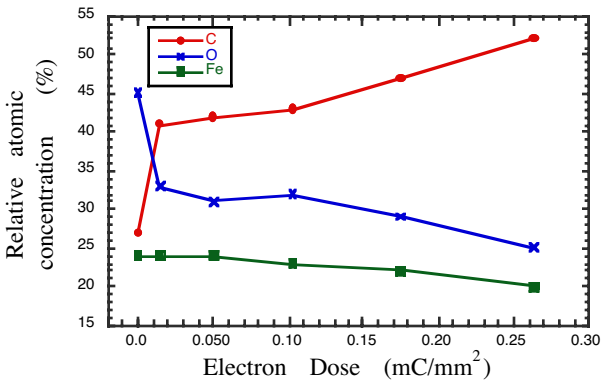

Figure 5: Surface C, O and Fe atomic concentrations as a function of multipacting electron dose, courtesy of D.Latorre.

3.4 The effect of an external solenoid field

The effect of an external solenoid field on the electron cloud during multipacting has been studied by passing a current through a wire coiled around the vacuum chamber. Multipacting triggered by pulse amplitudes of 210 V and 195 V can be completely suppressed with a solenoid field of 4.7 Gauss and 3.5 Gauss. Previous studies indicated that a solenoid field of 50 Gauss was sufficient to inhibit multipacting in a similar apparatus [21]. However, neither the effect of a strong dipole field (7.5 T) nor a superimposed solenoid field was effective in suppressing multipacting.

4 OUTLOOK

A number of the electron cloud key parameters, addressed in this paper, have been quantified by studies in the laboratory on the LHC prototype beam screen material, namely OFE Cu co-laminated on to a high-Mn content stainless steel. These studies are on–going and are being extended to other technical materials to be used in regions of the machine other than in the arcs, such as the long straight sections and experimental beampipes. In addition, information such as diffuse photon reflection, effects at cryogenic temperatures, secondary electron yield dependence on photon scrubbing, electron reflectivity, etc are presently being sought.

With the recent advent of a LHC–like proton beam (25 ns bunch spacing but with a total intensity of $6{\cdot}10^{12}$ protons in 81 bunches) in the SPS at CERN, multipacting studies may commence on a real accelerator. Indeed, very recent studies with the LHC–like beam in the SPS exhibited very fast pressure rises most probably due to electron stimulated desorption caused by electron multipacting [22].

5 REFERENCES

[1] "Beam induced multipacting."
O.Gröbner.
10th International conference on high energy accelerators, Protvino, July 1977.

[2] "A simulation study of electron-cloud instability and beam–induced multipacting in the LHC"
F.Zimmermann.
CERN LHC Project Report 95 (1997)

[3] "Beam induced multipacting."
O.Gröbner.
CERN LHC Project Report 127 (1997)

[4] "Simulations for the beam-induced electron cloud in the LHC beam screen with magnetic field and image charges."
O.S.Brüning.
CERN LHC Project Report 158 (1997)
and
"Numerical simulations for the beam–induced electron cloud in the LHC."
O.S.Brüning.
CERN LHC Project Report 190 (1998)

[5] "The electron–cloud effect in the arc of the LHC."
M.A.Furman.
CERN LHC Project Report 180 (1998)

[6] "Beam–induced electron cloud in the LHC and possible remedies."
V.Baglin, C.Benvenuti, O.Brüning, R.Calder, F.Caspers, I.R.Collins, O.Gröbner, N.Hilleret, B.Jeaneret, J–M.Laurent, M.Morvillo and F.Ruggiero.
CERN LHC Project Report 188 (1998)

[7] "Electron Cloud in the LHC."
F.Ruggiero.
http://wwwslap.cern.ch/collective/electron-cloud/.

[8] "Electron cloud in the LHC."
F.Ruggiero.
CERN LHC Project Report 166 (1998)

[9] "Photon reflection and photoelectron yield measurements in EPA."
V.Baglin, I.R.Collins and O.Gröbner.
CERN Vacuum Technical Note, in preparation (1999)

[10] "Reflection of photons and azimuthal distribution of photoelectrons in a cylindrical beam pipe."
V.V.Anashin, O.B.Malyshev, N.V.Dedorov, V.P.Nazmov, B.G.Goldenberg, I.R.Collins, O.Gröbner.
CERN LHC Project Report 266 (1999)

[11] "Azimuthal distribution of photoelectrons for a LHC beam screen prototype in a magnetic field."
V.V.Anashin, O.B.Malyshev, N.V.Federov and A.A.Krasnov.
CERN Vacuum Technical Note 99–06 (1999)

[12] "Photoelectron current in a magnetic field."
V.V.Anashin, R.V.Dostovalov, A.A.Krasnov, O.B.Malyshev and E.E.Pyata.
CERN Vacuum Technical Note 99–03 (1999)

[13] "The effect of the temperature and of a thick layer of condensed CO_2 on the photoelectron emission and on the photon reflection."
V.V.Anashin, A.A.Krasnov, O.B.Malyshev and E.E.Pyata.
CERN Vacuum Technical Note 99–05 (1999)

[14] "Photoelectron current from a substrate with cryosorbed gases."
V.V.Anashin, O.B.Malyshev and E.E.Pyata.
CERN Vacuum Technical Note 99–04 (1999)

[15] "VUV synchrotron radiation photoemission investigation of proposed materials from the vacuum chambers of the Large Hadron Collider."
I.R.Collins A.G.Mathewson and R.Cimino.
CERN Vacuum Technical Note 97–24 (1997)

[16] "VUV photoemission studies of candidate Large Hadron Collider vacuum chamber materials."
R.Cimino, I.R.Collins and V.Baglin.
Physical Review Special Topics – Accelerators and Beams, **2**, 063201 (1999)

[17] "Photon scrubbing studies in EPA of OFE Cu, a LHC prototype beam screen material."
V.Baglin, I.R.Collins, O.Gröbner and J.Gómez-Goñi.
CERN Vacuum Technical Note, in preparation (1999)

[18] "Photon–stimulated desorption yields from stainless steel and copper–plated beam tubes with various pretreatments."
C.L.Foerster, H.Halama and C.Lanni,
J. Vac. Sci. Technol., **A8**, 2856 (1990)

[19] "Electron cloud and beam scrubbing in the LHC."
O.Brüning, F.Caspers, I.R.Collins, O.Gröbner, B.Henrist, N.Hilleret, J–M.Laurent, M.Morvillo, M.Pivi, F.Ruggiero and X.Zhang.
CERN LHC Project Report 290 (1999)

[20] "Freon Plasma surface treatment for multipactoring."
J.W. Noé.
Nuclear Instruments and Methods, **A328** 291 (1993)

[21] "Multipacting tests with magnetic field for the LHC beam screen."
O.Brüning, F.Caspers, J–M.Laurent, M.Morvillo and F.Ruggiero.
CERN LHC Project Report 187 (1998)

[22] J.M.Jimenez, private communication